*Contemporary Physics*, 2015
Vol. 56, No. 1, 2–16, http://dx.doi.org/10.1080/00107514.2015.971625

Taylor & Francis
Taylor & Francis Group

# Nature's optics and our understanding of light

M.V. Berry*

*H H Wills Physics Laboratory, University of Bristol, Bristol BS8 1TL, UK*

(*Received 8 September 2014; accepted 23 September 2014*)

Optical phenomena visible to everyone have been central to the development of, and abundantly illustrate, important concepts in science and mathematics. The phenomena considered from this viewpoint are rainbows, sparkling reflections on water, mirages, green flashes, earthlight on the moon, glories, daylight, crystals and the squint moon. And the concepts involved include refraction, caustics (focal singularities of ray optics), wave interference, numerical experiments, mathematical asymptotics, dispersion, complex angular momentum (Regge poles), polarisation singularities, Hamilton's conical intersections of eigenvalues ('Dirac points'), geometric phases and visual illusions.

**Keywords:** refraction; reflection; interference; caustics; focusing; polarisation



## 1. Introduction

Natural optical phenomena have been the subject of many studies over many centuries, and have been described many times in the technical [1,2] and popular [3–5] literature. Yet another general presentation would be superfluous. Instead, as my way of celebrating the International Year of Light, this article will have a particular intellectual emphasis: to bring out connections between what can be seen with the unaided, or almost unaided, eye and general explanatory concepts in optics and more widely in physics and mathematics – to uncover the arcane in the mundane. In addition, I will make some previously unpublished observations concerning several curious optical effects.

Each section will describe a particular phenomenon, or class of phenomena, which I try to present in the simplest way compatible with my theme of underlying concepts. The sections are almost independent and can be read separately.

A disclaimer: The historical elements in what follows should not be interpreted as scientific history as practised by professionals, where it is usual to study the contributions of scientists in the light of the times in which they lived. My approach is different: to consider the past in the light of what we know today – for the simple reason that the scientific contributions we remember are those that have turned out to be fruitful in later years or even (as we will see) later centuries. The significance of the past changes over time.

## 2. Rainbows: the power of numerical experiments

Figure 1 is Roy Bishop's photograph of a primary rainbow accompanied by a faint secondary bow. It is iconic because the house in the picture is Isaac Newton's birthplace and it was Newton who gave the first explanation of the rainbow's colours [6]. We will see later why the picture is ironic as well as iconic.

To a physicist, the colours are a secondary feature, associated mainly with the dependence of refractive index of water on wavelength (optical dispersion). More fundamental is the very existence of a bright arc in the sky. This had been explained by Descartes in 1638 [7]. To calculate the paths of light rays (Figure 2(a)) refracted into and out of a raindrop, with one reflection inside, he used the law of refraction that he probably discovered independently, though we associate it with Snel, who knew it already (and it was known to Harriot several decades before, and to Ibn Sahl half a millennium earlier [8]).

Nowadays, we would use elementary trigonometry to find the deviation $D$ of a ray incident on the drop with impact parameter $x$, if the refractive index is $n$:

$$D(x) = \pi - \left(4\sin^{-1}\frac{x}{n} - 2\sin^{-1}x\right). \tag{1}$$

The calculation reveals a minimum deviation (Figure 2(b)) given by

$$\frac{\mathrm{d}D}{\mathrm{d}x} = \frac{2\left(\sqrt{1-x^2} - 2\sqrt{n^2-x^2}\right)}{\sqrt{(1-x^2)(n^2-x^2)}} = 0 \quad \text{for } x = x_{\min} = \sqrt{\frac{4-n^2}{3}}, \tag{2}$$

corresponding to the deviation of the rainbow ray, namely

*Email: asymptotico@bristol.ac.uk

Figure 1. Rainbow over Isaac Newton's birthplace, showing the primary bow decorated by a supernumerary bow, and a faint secondary bow. Reproduced by kind permission of Professor Roy Bishop.

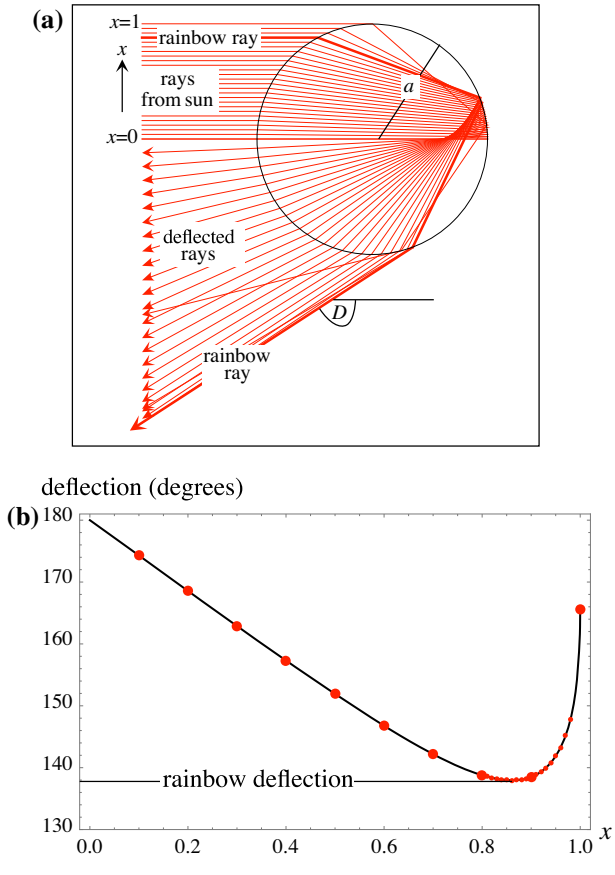


Figure 2. (a) Rays in a raindrop; showing the minimum deviation (rainbow) ray. (b) Ray deflection function, with dots indicating the points calculated by Descartes.

$$D_{\min} = D(x_{\min}) = 2\cos^{-1}\left(\frac{(4-n^2)^{3/2}}{3^{3/2}n^2}\right)$$
$$= 180^\circ - 42.03^\circ \text{ for } n = \frac{4}{3}. \quad (3)$$

Descartes proceeded differently. Our facility with trigonometric calculations was not available in his time; instead, he used a geometric version of Snel's law to compute the rays laboriously, one by one. As we would say now, he performed a *numerical experiment*. The dots in Figure 2(b) correspond to the rays he calculated [7].

But why should the rainbow ray, emerging at $D_{\min}$, be bright? What about the other, more deviated, rays, illuminating the sky inside the bow? Descartes understood that although the drop is lit uniformly in $x$, the rays emerge non-uniformly in $D$. In particular, rays incident in an interval d$x$ near $x_{\min}$ emerge concentrated into a range d$D = 0$. This is *angular focusing*: a lot goes into a little. The rays emerge as a *directional caustic*. The rainbow caustic is a bright cone emerging from each droplet; and we, looking up at the rain, see, brightly lit, in the form of an arc, all the drops on whose cones our eyes lie. We will encounter the concept of a caustic repeatedly in later sections of this paper; it denotes the envelope of a family of rays, that is the focal line or surface touched by each member of the family. A caustic is a holistic property of a ray family, not inherent in any individual ray. Caustics are the singularities of geometrical optics [9].

The intensity $I$ corresponding to deviation $D$, given by equating the light entering in an annulus around $x$ and emerging in a solid angle around $D$, is

$$|2\pi \sin D \mathrm{d}D| I \propto |2\pi x| \mathrm{d}x, \text{ i.e. } I \propto \left|\frac{x}{\sin D}\left(\frac{\mathrm{d}D}{\mathrm{d}x}\right)^{-1}\right|. \quad (4)$$

This diverges at the rainbow angle (3), predicting, on this geometrical-optics picture, infinite intensity where d$D$/d$x = 0$. The singularity would be softened by the 1/2° width of the sun's disc and the colour dispersion.

Now look more closely at Figure 1, and notice the bright line just inside the main arc. This *supernumerary bow* did not fit into the Newton–Descartes scheme, and there seems no evidence that Newton noticed it (the term 'supernumerary means 'surplus to requirements', i.e. 'unwanted'). The explanation had to wait for nearly a century, when Young [10–12] pointed out, as an example of his wave theory of light, that supernumerary bows are *interference fringes*, resulting from the superposition of the waves associated with the two rays that emerge in each direction $D$ away from the minimum. It is remarkable that just by looking up in the sky at this fine detail (visible in about half of natural rainbows), one sees directly the replacement of the theory of light in terms of rays – geometrical optics – by the deeper and more

fundamental wave theory. This is the irony of Figure 1: interference fringes, that Newton could not explain, hovering over his house, as if in mockery.

Young understood that his two-wave picture could not be a precise description of the light near a rainbow because the intensity would still diverge at the rainbow angle, and he had the insight that – using modern terminology – a wave should be described by a smooth wave function. It took nearly 40 years for Airy [13] to provide the definitive formula for the smooth wave function near a caustic. He calculated that the intensity (Figure 3(a)) is the square of an integral, now named after him:

$$\mathrm{Ai}(x) = \frac{1}{\pi}\int_0^\infty \mathrm{d}t \cos\left(\frac{1}{3}t^3 + xt\right). \tag{5}$$

For light wavelength $\lambda$ and a drop with radius $a$, the 'rainbow-crossing variable' $x$ is [14]

$$x = (D_{\min} - D)\left(\frac{4\pi a}{3\lambda}\right)^{2/3} \frac{\sqrt{n^2-1}}{(4-n^2)^{1/6}}. \tag{6}$$

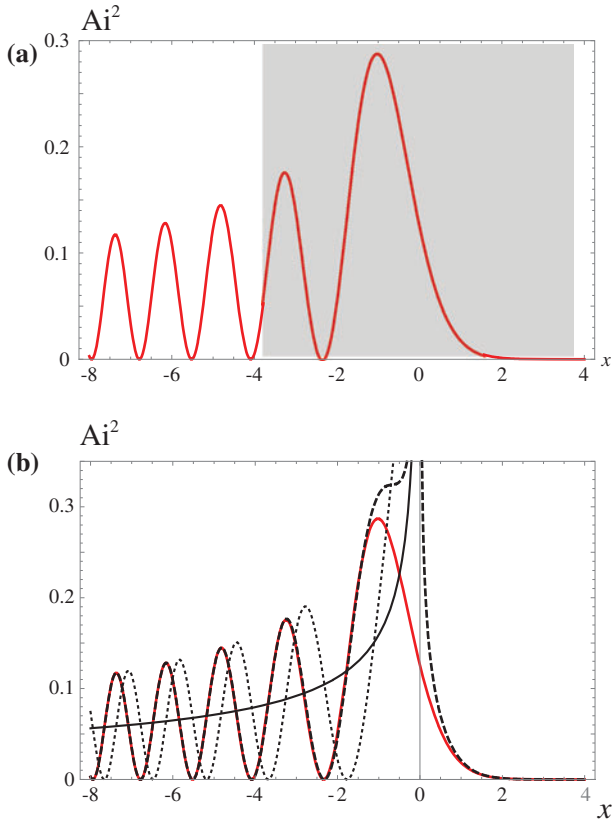


Figure 3. (a) Airy function intensity, with shading indicating the range that Airy computed by numerical integration. (b) Red curve: Airy intensity; black curve: geometrical optics approximation; dotted curve: Young's interfering ray approximation; Dashed curve: lowest-order Stokes asymptotics.

Airy realised that Ai($x$) describes the wave close to any caustic, not just that associated with a rainbow.

Notwithstanding repeated attempts to understand (5), Airy did 'not succeed in reducing it to any known integral'. Therefore, he resorted to what Descartes had done two centuries before and what we continue to do today when faced with a mathematically intractable theory. He performed a *numerical experiment*: evaluating the integral by approximate summation of the integrand in increments d$t$ – a far from trivial task given the oscillatory nature and slow convergence. The result was that he could calculate Ai($x$) over the range $|x| < 3.748$ shown shaded on Figure 3(a) [13], including just two peaks of $\mathrm{Ai}^2(x)$.

This restriction to barely two intensity maxima was frustrating, because 30 supernumerary fringes had been observed in laboratory experiments with transparent spheres. What was lacking was the *asymptotics* of Ai($x$): a precise description of the oscillations for $x \ll -1$ and the decay into the geometrically forbidden region $x \gg +1$. This was supplied 10 years later by Stokes [15], who showed that (Figure 3(b))

$$\frac{\cos\left(\frac{2}{3}(-x)^{3/2} + \frac{1}{4}\pi\right)}{\sqrt{\pi}(-x)^{1/4}} \underset{x\ll -1}{\leftarrow} \mathrm{Ai}(x) \underset{x\gg 1}{\leftarrow} \frac{\exp\left(-\frac{2}{3}x^{3/2}\right)}{2\sqrt{\pi}x^{1/4}}. \tag{7}$$

Stokes's paper was technically remarkable; using the differential equation satisfied by Ai($x$), he 'pre-invented' what later came to be known as the WKB method and, to identify certain constants, he anticipated the method of stationary phase for oscillatory integrals. But his insight was far deeper, leading him to identify a difficulty and contribute to its solution, in a way that has proved central to contemporary mathematics.

The asymptotics (7) shows that for $x \gg +1$, Ai($x$) is described by one exponential function, while for $x \ll -1$, there are two exponentials (because $\cos\theta = (\exp(\mathrm{i}\theta) + \exp(-\mathrm{i}\theta))/2$). One of these is the analytic continuation, through complex $z = x + \mathrm{i}y$, of the exponential for $x \gg +1$. But where did the other come from? The key was identified by Stokes a further decade later [16,17]: the exponentials in (7) are the first terms in formally exact expressions as *divergent infinite series*. For Re ($z$) $\gg +1$, i.e. on the dark side, the series is

$$\mathrm{Ai}(z) = \frac{\exp\left(-\frac{2}{3}z^{3/2}\right)}{2\sqrt{\pi}z^{1/4}} \sum_{n=0}^{\infty} (-1)^n \frac{\left(n-\frac{1}{6}\right)!\left(n-\frac{5}{6}\right)!}{2\pi n!\left(\frac{4}{3}z^{3/2}\right)^n}. \tag{8}$$

The divergence arises from the factorials: two in the numerator dominating one in the denominator. Nevertheless, for large $z$, the terms start by getting smaller, making the series practical for accurate numerical evaluation.

Stokes thought that the greatest accuracy is obtained by truncating the series at the least term (after which, the

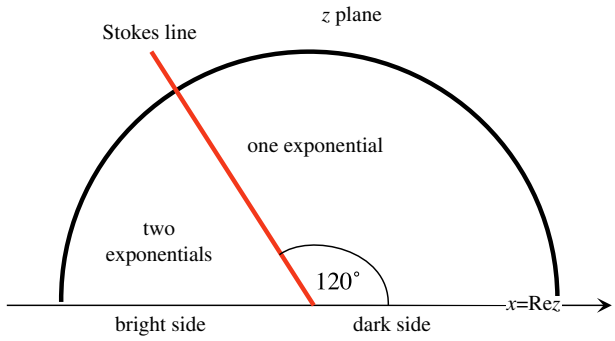


Figure 4. Complex plane of Ai($z$), with the Stokes line across which the second exponential is born.

series starts to diverge), leaving a small remainder representing an irreducible vagueness in the representation of Ai($z$) by the series. In a path in the upper $z$ half-plane from $z$ positive real to negative real (Figure 4), the small exponential on the right of (7) becomes exponentially large when arg$z$ = 120°. Near this 'Stokes line', the second exponential on the left of (7) is exponentially small – smaller, indeed, than the remainder of the truncated series, allowing it to enter Ai($z$) unnoticed and then to grow into the previously problematic oscillatory second exponential for $z$ negative real, giving the cosine interference fringes on the bright side of the rainbow.

Although Stokes was wrong in thinking that the accuracy of factorially divergent series is limited by the smallest term, his Stokes lines appear in a wide variety of functions and are seminal to our modern understanding of divergent series. We now know [18–21] that the second exponential is born from the resummed divergent tail of the series multiplying the first exponential, and in a manner that is the same for all factorially divergent series. This universality, first emphasised by Dingle [22], enables repeated resummation and computation of functions with unprecedented accuracy [23,24]. The associated technicalities are now being applied in quantum field theory and string theory [25].

We see that understanding the rainbow has been an intellectual thread linking numerical experimentation, evidence for wave optics superseding ray optics and the mathematics of divergent series.

This far from exhausts the physics associated with the rainbow. The $\lambda$ dependence of the rainbow Airy argument (6) contributes diffraction colours [26] in addition to the dispersion colours explained by Newton [7]. The electromagnetic vector nature of light explains subtle polarisation detail [14]. The function Ai($x$), that in its original form, e.g. with the variable (6), describes only the close neighbourhood of a caustic, can be stretched to provide a *uniform approximation* [27–29] extending the accuracy to regions far from the caustic. Analogues of rainbow scattering occurs in quantum [28,30,31] and condensed matter [32] physics. Finally, Ai($x$) is now understood as the simplest member of a hierarchy of *diffraction catastrophes* [9,33,34], describing waves near caustics of increasing geometrical complexity.

## 3. Sparkling seas: twinkling and lifelong fidelity

Figure 5 shows images of the sun reflected by wavy water. The images we see correspond to places where the water surface is sloped to reflect light into our eye. As the waves move and the shape of the surface changes, the images move too. They appear and disappear in pairs. Such events, called 'twinkles', correspond to caustic surfaces (Figure 6(a)) in the air above the water, passing through the eye. The succession of twinkles, often too rapid for us to follow in detail, gives rise to the sparkling appearance of the water. The intricate topology of the reflections and the coalescence events, and the associated statistics for waves represented by Gaussian random functions were studied in pioneering papers by Longuet-Higgins [35–37]. The techniques he developed were applied to the statistics of caustics [9] and extended to describe phase [38] and polarisation singularities [39] in random waves.

Here, I draw attention to a statistical problem hinted at by Longuet-Higgins [35,37] but still unsolved. Each specular point is born accompanied by a partner, prompting this question: For a random moving water surface, what fraction $R$ of specular points dies by annihilation with the partner it was born with? This property can be called 'lifelong fidelity'. The fraction $R$ is different for different types of randomness. It seems a hard problem even for the simple case of isotropic monochromatic

Figure 5. Images of the sun (specular points) sparkling on the water in Bristol docks.

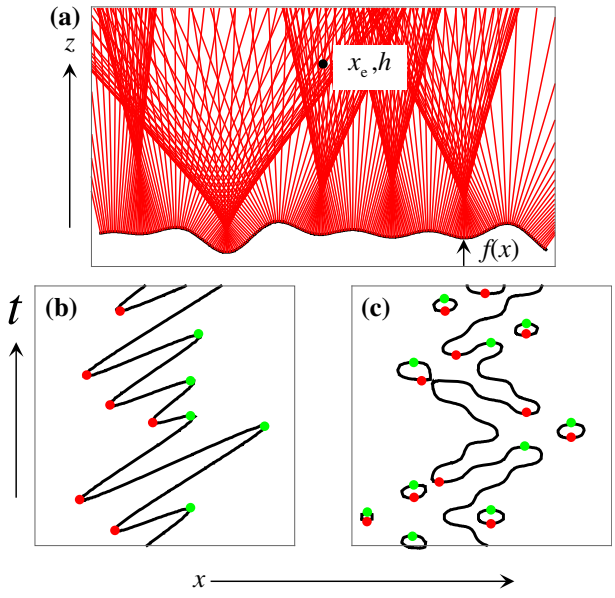


Figure 6. (a) Reflection caustics above a water surface (13). (b) Space–time plot of evolving images, for the rigidly moving surface (14), with births of image pairs indicated by red dots and deaths by green dots; (c) As (b) for the interfering waves (15), with the loops indicating images enjoying lifelong fidelity.

Gaussian randomness, because it requires statistics non-local in both space and time.

To get a little insight, I illustrate the problem by considering the simpler case of a corrugated water surface generating a reflected wavefront with height $f(x)$ depending on a single variable $x$ (the height of the water surface is proportional to $f(x)$). For the eye located at $(x_e, h)$, the optical path distance from a point $x$ on the water surface is (for surfaces with gentle slopes),

$$\Phi(x;x_e,h,t)=\sqrt{(h-f(x,t))^2+(x-x_e)^2}\approx h-f(x,t)+\frac{(x-x_e)^2}{2h}. \tag{9}$$

The specular points $x_n$, i.e. the rays, are the paths for which this function is stationary:

rays:
$$\partial_x\Phi=0\Rightarrow x-hf'(x,t)=x_e\Rightarrow x=\{x_n(x_e,h,t)\}. \tag{10}$$

Therefore, the moving images are represented by the locus

$$x-hf'(x,t)=x_e \tag{11}$$

in the $(x, t)$ plane. The caustics at time $t$ are the curves

$$\partial_x^2\Phi=0\Rightarrow z=\frac{1}{f''(x,t)}\Rightarrow z(x_e,h,t). \tag{12}$$

To illustrate lifelong fidelity, or lack of it, I start with a stationary surface given by a random superposition of $N$ sinusoids:

$$f_0(x)=\sum_{n=0}^{N}\cos(k_nx+\phi_n). \tag{13}$$

Figure 6(a) illustrates the caustics for a sample function of this type, with $N = 5$. If the water moves rigidly, represented by

$$f_1(x,t)=f_0(x-t), \tag{14}$$

then the caustics translate rigidly sideways and it is obvious that there is no lifelong fidelity (Figure 6(b)). Non-rigid motion can be represented by two interfering oppositely moving waves:

$$f_2(x,t)=\frac{1}{2}(f_0(x-t)+f_0(x+t)). \tag{15}$$

Now, some of the caustics move back and forth or up and down, and most images enjoy lifelong fidelity (closed loops in Figure 6(b)); for a single sinusoid ($N = 1$), *all* caustics in $f_2(x, t)$ move up and down and lifelong fidelity is universal.

For the two-dimensional case, Longuet-Higgins presents a time exposure showing paths of specular points on the water surface [35]. Some of the paths are closed loops, but in contrast to the space–time plots in the corrugated case, these do not always correspond to lifelong fidelity. This is a rich subject for further analytical study and numerical experiment.

## 4. Mirages, green flashes: light bent and dispersed by air

Air bends light. One consequence, again involving caustics in an essential way, is the mirage, most commonly seen on a hot day when distant cars appear reflected from the surface of a long, straight road. As is well known [3,4,40], this is really refraction masquerading as reflection: bending by the gradient of refractive index, increasing from the hot road surface to the cooler air above (Figure 7).

On the simplest theory, the index depends weakly on height $z$:

$$n(z)=1+\Delta n(z),\quad \Delta n(z)\ll 1. \tag{16}$$

From Snel's law, the direction and curvature of a ray are given by

$$n(z)\cos(\theta(z))=n(z_{\min})\Rightarrow z''(x)\approx\Delta n'(z), \tag{17}$$

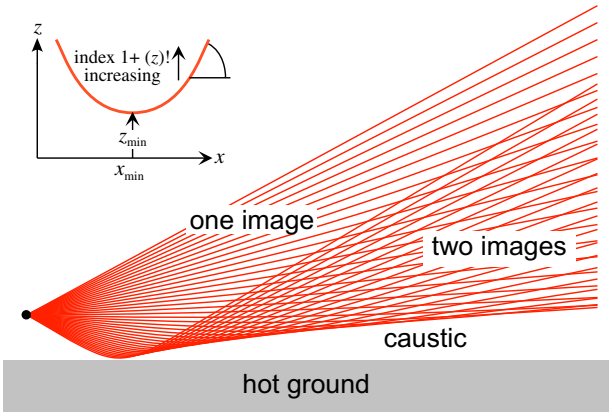


Figure 7. Mirage rays (20) for the monotonic index profile (20).

where $z_{min}$ is the height where the ray is horizontal. For constant index gradient, i.e. $n(z)$ locally linear, this leads to parabolic ray paths:

$$\Delta n(z) = Az \Rightarrow z = z_{min} + \frac{1}{2}A(x - x_{min})^2. \qquad (18)$$

(A curious sidelight on history: this simple explanation has been challenged several times over more than two centuries, on the grounds, based on a misunderstanding of Snel's law, that once a ray becomes horizontal, it could never curve upwards again [41].)

Figure 7 shows the family of ray paths from a point source, with a more realistic index function, increasing from $1 + \Delta_0$ at the ground to $1 + 2\Delta_0$ above:

$$\Delta n(z) = \Delta_0\left(2 - \exp\left(-\frac{z}{L}\right)\right). \qquad (19)$$

The rays can be determined analytically:

$$x - x_{min} = \frac{1}{\sqrt{2\Delta_0}}\exp\left(-\frac{z_{min}}{L}\right)\times \left(z - z_{min} + 2L\log\left(1 + \sqrt{1 - \exp\left(-\frac{z - z_{min}}{L}\right)}\right)\right) \qquad (20)$$

Each ray from the source corresponds to a different choice of $x_{min}$ and $z_{min}$ determined by its initial slope. The caustic of the family is clearly visible. It separates eye positions below the caustic, from which the source is invisible, from positions above, where two images can be seen. (Some rays from the source hit the ground, giving rise to an additional boundary in Figure 7: a shadow edge separating the two-image region above the caustic from a one-image region higher still.)

The caustic has a further significance. Each point of a distant object emits its own family of rays, so the complete object emits a family of families of rays. With the eye in a fixed position, the parts of the object that can be seen, bounded below by the 'vanishing line', are those whose caustics lie below the eye.

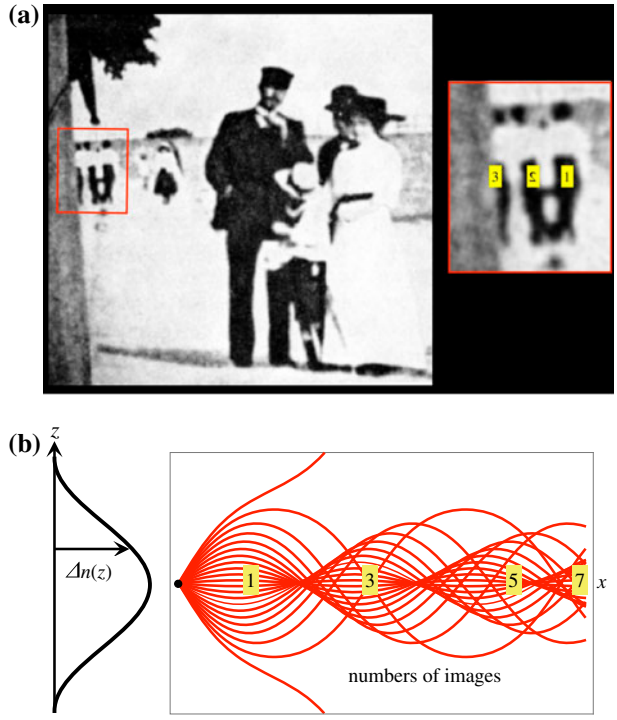


Figure 8. (a) Mirage with three images, formed by refraction near a hot wall (adapted from W. Hillers, *Phys. Z.* 14 (1913), 719–723, reproduced in [3]). (b) Mirage rays (22) in a duct, for the index profile (21) possessing a maximum.

Sometimes, more than two mirage images are visible; Figure 8(a) shows a case where there are three [3]. Such multiple images can arise when the index is not a monotonic function of height, or from undulations of the surface; refractive indices with a maximum generate a duct, where in principle any number of images can be seen. A solvable example is

$$\Delta n(z) = A\cos\left(\tfrac{z}{a}\right) \Rightarrow z''(x) = -\tfrac{A}{a}\sin\left(\tfrac{z(x)}{a}\right) \quad \{|z| < a\pi,\ z(0) = 0,\ z'(0) \equiv \theta_0\}, \qquad (21)$$

for which, the rays, illustrated in Figure 8(b), involve the Jacobian elliptic functions sn and am [42]:

$$z(x) = 2a\sin^{-1}\mathrm{sn}\left(\frac{x\theta_0}{2a}\middle|\frac{2\sqrt{A}}{\theta_0}\right) = 2a\,\mathrm{am}\left(\frac{x\theta_0}{2a}\middle|\frac{2\sqrt{A}}{\theta_0}\right). \qquad (22)$$

For more on the topology of images, see [43,44].

Mirages involve local bending of light, with the layer of heated air a few centimetres high and horizontal distances of a few hundred metres. On a much larger scale, the entire atmosphere of the spherical earth can be

regarded as a lens, with index decaying to unity over a height of a few kilometres. The resulting bending elevates the image of the sun by slightly more than its own diameter (about 1/2°), so we can see it immediately before sunrise and after sunset, when it is just below the horizon.

The earth-lens suffers from chromatic aberration because the bending is weakly dispersive, with the blue being refracted more than the red. This causes the green image of the setting sun to be above the red image by about 10 arcsec, giving rise to the occasionally visible striking phenomenon of the green flash [45,46] (the blue sunlight has been scattered to make the blue sky). Important modifications of this basic explanation arise from the fact that the dispersion need not be a monotonic function of height (e.g. when there is an inversion layer) [46].

More effects of the earth-lens will be examined in the next section.

## 5. Earthlight on the moon: astronomical coincidences

There are two circumstances in which we see the moon lit from the earth. Near new moon (Figure 9(a)), the part of the moon's disc that is hidden from the sun can be seen in the pale ghostly light reflected by the earth – also called 'earthshine' or 'the old moon in the new moon's arms'. And in the opposite situation, during a lunar eclipse, the moon can still be seen, even though it is within the earth's shadow, in light refracted onto it by the earth's atmosphere (Figure 9(b)). This eclipse light corresponds to all the simultaneous sunrises and sunsets on the earth, blood-reddened by double passage through the atmosphere.

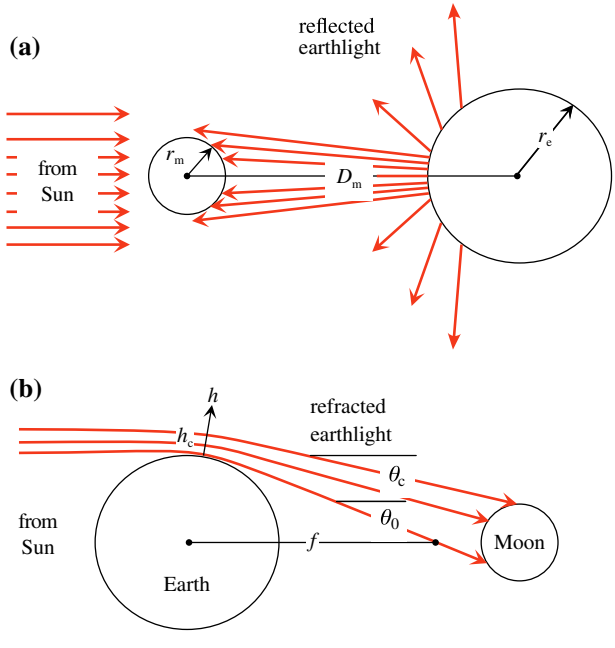


Figure 9. (a) The old moon in the new moon's arms: earthlight reflected onto the moon at new moon. (b) earthlight refracted onto the moon during a lunar eclipse.

These two earthlights are of very different origins. Nevertheless, casual viewing suggests that the brightness of the earth-lit moon is roughly similar in the two cases. In this section, I outline calculations supporting this observation.

At new moon, the sun illuminates the disc of the earth that faces the moon. The earth's albedo $A$ denotes the fraction of this light that is diffusely reflected into (approximately) a hemisphere of the sky. Most of it disappears into space, but a small fraction hits the moon. Neglecting obliquity effects, the fraction of sunlight incident on the earth that lights up the new moon is (Figure 9(a))

$$F_{\text{new}} = A\frac{\pi r_{\text{m}}^2}{2\pi D_{\text{m}}^2} = \frac{A r_{\text{m}}^2}{2D_{\text{m}}^2}. \tag{23}$$

During a lunar eclipse, the sunlight reaching the moon corresponds to a thin annulus of height $h_c$, below which rays passing close to the earth's surface are bent onto the moon (Figure 9(b)). During its passage through the atmosphere, this light is attenuated by a factor $\alpha$. Thus, the fraction of incident sunlight that lights up the eclipsed moon is

$$F_{\text{eclipse}} = \alpha\frac{2\pi h_{\text{c}} r_{\text{e}}}{\pi r_{\text{e}}^2} = \frac{2\alpha h_{\text{c}}}{r_{\text{e}}}. \tag{24}$$

We need to calculate the ratio of these two earthlights, namely

$$R \equiv \frac{F_{\text{new}}}{F_{\text{eclipse}}} = \frac{A r_{\text{m}}^2 r_{\text{e}}}{4\alpha h D_{\text{m}}^2}. \tag{25}$$

Some of the required numbers are

$$\begin{aligned} &r_{\text{e}} = 6371\,\text{km},\ r_{\text{m}} = 1737\,\text{km},\\ &D_{\text{m}} = 384{,}000\,\text{km},\ A \sim 0.3. \end{aligned} \tag{26}$$

In addition, we need $h_c$ and $\alpha$.

To calculate $h_c$, we need the angular deflection of sunrays passing the earth at height $h$ above the ground. This can be calculated from Snel's law, but it is simpler to use the observed deviation $\theta_0$ of a ground-grazing ray (twice the elevation of the setting sun) and assume an exponential atmosphere with scale height $H$. Thus

$$\theta(h) = \theta_0 \exp\left(-\frac{h}{L}\right),\ L = 8\,\text{km},\ \theta_0 = 1.18^\circ = 0.0206. \tag{27}$$

An interesting related fact (apparently first noticed by John Herschel) is that the focal length of the earth-lens, determined by the distance from the earth that a grazing ray crosses the sun–earth axis, is relatively close to the moon:

$$f = \frac{r_e}{\theta_0} = 309{,}349\,\text{km} = D_m - 74{,}650\,\text{km}. \tag{28}$$

It is easy to show that this grazing ray hits the moon after crossing the axis at the focus. Non-grazing rays do not cross at the focus (the earth-lens has powerful spherical aberration), and $h_c$ is determined by the deflection which hits the moon's edge (Figure 9(b)):

$$\theta_c = \frac{r_e - r_m}{D_m} \Rightarrow h_c = L \log\left(\frac{\theta_0 D_m}{r_e - r_m}\right) = 4.28\,\text{km}. \tag{29}$$

The final number we need is the attenuation $\alpha$. This is the square of the attenuation of the setting sun, namely the brightness of the setting sun relative to the unattenuated (roughly noonday) sun. We know it is a small number because we can gaze at the setting sun but not the noonday sun. $\alpha$ is small, but it is not zero, indicating (if proof were needed) that the earth is not flat: if it were, the sun setting over the faraway edge of the world would be invisible.

In reality, $\alpha$ is enormously variable and involves both scattering and absorption. But we can estimate it from first principles using the following formula for the ground-level attenuation per unit distance, resulting from scattering in clear air [47], in terms of $\lambda$, refractive index deviation $\Delta_0 = n - 1$ and the molecular particle density $N$:

$$\gamma_0 = \frac{2}{3\pi}\left(\frac{2\pi}{\lambda}\right)^4 \frac{{\Delta_0}^2}{N}. \tag{30}$$

Reasonable numbers give

$$\lambda = 5 \times 10^{-7}\,\text{m},\ \Delta_0 = 0.000292,\ N = 2.5 \times 10^{25}\,\text{m}^{-3} \Rightarrow \gamma_0 = 1.8 \times 10^{-2}\,\text{km}^{-1}. \tag{31}$$

Using this to calculate the exponential attenuation of a ray passing at height $h$ and averaging from $h = 0$ to $h = h_c$, gives

$$\alpha = \frac{1}{h_c}\int_0^{h_c} \mathrm{d}h \exp\left(-\gamma_0\sqrt{2\pi L r_e}\exp\left(-\frac{h}{L}\right)\right) = 6.8 \times 10^{-4} = (0.0261)^2. \tag{32}$$

(The square root 0.0261 is an estimate – apparently reasonable – of the attenuation of the setting sun: about 16 dB.)

Thus, finally we get, from (25), the ratio of earthlight intensities:

$$R = \frac{A r_m^2 r_e}{4\alpha D_m^2 L \log\left(\frac{\theta_0 D_m}{r_e - r_m}\right)} \sim 3.4. \tag{33}$$

This number should not be taken seriously as a precise estimate. But it does indicate that the two very different illuminations of the moon by the earth – at new moon from the brightly lit 'full earth' when most of the light is squandered into space, and during a lunar eclipse when the thin annulus of deflected light is efficiently focused onto the moon – are of comparable strengths. For an interesting related discussion of the visibility of the horizon at different heights, see [48].

## 6. The glory: focusing that vanishes geometrically

The optical glory is a halo around the shadow of an illuminated observer's head cast by the sun on a cloud or mist-bank (Figure 10). Nowadays, it is most commonly seen while flying in sunshine, looking down at the airplane's shadow on a cloud below. It took several centuries for this beautiful phenomenon to be fully understood [14,49], following its first recorded observation [4],

Figure 10. Glory around the shadow of the author's head on a cloud below Erice, Sicily, from light illuminating a temple in the village above.

because its explanation involves subtle connections between concepts usually regarded as separate.

First, note that since the glory appears at the edge of the observer's shadow on a cloud, it must be a back-scattering phenomenon associated with water droplets. It involves reflection from individual drops and so should not be confused with the much weaker Anderson localisation, which is back-scattering enhancement arising from the coherent interference of light multiply scattered by many droplets [50,51].

Imagine (counterfactually as it will turn out) that there is a light ray, incident non-axially (i.e. with finite impact parameter $x$) that enters the droplet, gets reflected once inside, and then emerges precisely backwards, i.e. with deflection $D(x) = \pi$ (Figure 11(a)). Rays near this $x$ will cross the symmetry axis, and associated with this rotational symmetry would be an entire ring of such rays, giving rise to focusing in the backward direction [47]: an *axial caustic*, represented by the singularity from $1/\sin D$ in (4) when $D = \pi$. It follows from (1) that such a ray exists with impact parameter $x$ if the index $n$ is

$$D(x) = \pi \Rightarrow n(x) = \frac{x\sqrt{2}}{\sqrt{1-\sqrt{1-x^2}}}. \qquad (34)$$

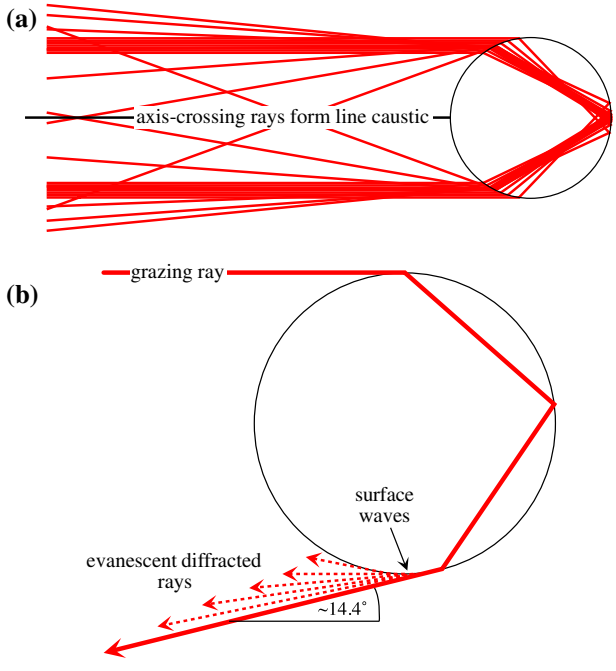


Figure 11. (a) Rays emerging backwards from a transparent sphere with index $n = 1.7$, and crossing the symmetry axis to form a focal line. (b) Diffracted rays creeping round the surface of a water droplet, generating the dominant contribution to the glory when they cross the symmetry axis.

As $x$ increases from 0 to 1, $n(x)$ decreases from 2 to $\sqrt{2}$. But the refractive index of water, approximately 4/3, lies outside this range, so there are no axis-crossing rays: the glory enhancement cannot be explained as a focusing effect within geometrical optics. (Backward ray focusing from spheres of glass or plastic with indices in the range $\sqrt{2} < n < 2$, finds application in retro-reflecting paint.)

To understand the true mechanism of nature's glory, we note that although the rays do not reach the backward direction for water, they get close. For the grazing rays, with $x = 1$, the deflection is

$$D(x=1) = \pi - \left(4\sin^{-1}\left(\frac{1}{n}\right) - \pi\right)$$
$$\Rightarrow 180^\circ - 14.36^\circ \text{ if } n = \frac{4}{3}. \qquad (35)$$

To accommodate the 14° shortfall, some of the emerging light gets trapped into a *surface wave* that creeps around the surface of the droplet, radiating tangentially while doing so (Figure 11(b)) and reaching $D = 180^\circ$ and beyond. These axis-crossing evanescent surface waves form the backward caustic and contribute to the glory. According to this mechanism, the back-scattered intensity $I_b$, for light wavelength $\lambda$ and drop radius $a$, is [14,49]

$$I_b \sim \left(\frac{a}{\lambda}\right)^{8/3} \exp\left(-\text{constant}\left(\frac{a}{\lambda}\right)^{1/3}\right), \qquad (36)$$

in which the first factor describes axial focusing, the exponential represents the decay as the creeping wave skips the 14° while radiating, and the powers 1/3 come from the fact that the surface is a caustic of the creeping waves.

A full analysis of electromagnetic waves scattered from transparent spheres [49,52] reveals great complexity beyond the creeping-and-focusing picture. This includes: waves skipping many times inside the drop before emerging, causing high-order backward rainbows; very fine angle- and size-dependent interference oscillations; and delicate polarisation effects. But the exponential angular decay is a dominant feature, described analytically in terms of *complex angular momentum*: an unexpected application to this natural phenomenon of the *Regge poles* (complex angular-momentum singularities) devised to explain the quantum scattering of elementary particles.

From (36), we see that the intensity vanishes for large droplets because the focusing enhancement is cancelled by the evanescence (decay during the 14° skip) and also for very small droplets, where the focusing is softened by diffraction. That is why the glory is observed in the small droplets occurring in clouds or mist, but not in rain where the droplets are bigger.

Summing up: *the glory is a focusing effect that vanishes in the geometrical-optics limit*.

## 7. Hidden daylight: polarisation singularities in the sky

A fundamental aspect of light waves is that they are electromagnetic. Therefore, they can be polarised. But we (unlike some other animals) possess only the most rudimentary perception of polarisation, blinding us to a beautiful polarisation pattern decorating the daylight sky above us [53]. Although sunlight arrives unpolarised, the Rayleigh (dipole) scattering from air molecules that is responsible for the blue sky induces polarisation [3]. Scattered sunlight is strongly polarised perpendicular to the sun (as can immediately be verified with a polarising sheet), whereas forward and back-scattered sunlight remains unpolarised.

If sunlight were scattered only once, daylight would be unpolarised in the direction of the sun and in the opposite direction, namely the anti-sun (visible before sunrise and after sunset). But in reality, the number of unpolarised points (directions) in the sky is not two, but four: several degrees above and below the sun and the anti-sun. Three were observed in the nineteenth century and the fourth, below the anti-sun, was seen only recently, from a balloon [54]. The reason for four is that each single-scattering unpolarised direction is split into two by multiple scattering.

The sky is decorated by a pattern of polarisation directions (e.g. of the electric vector of daylight) organised by these four points, only two of which are visible at any time. Figure 12(a) shows the pattern at a time when the sun is in the indicated position. The key to understanding it, discovered only relatively recently [55] by emphasising something lacking in a tradition of elaborate multiple-scattering theory [56–58], is geometric: the realisation that the unpolarised points are *polarisation singularities*: places where the direction of polarisation is undetermined.

Near each singularity, the geometry is that of a 'fingerprint', around which the polarisation direction turns by 180°. The turn is 180°, rather than 360°, because a half-turn leaves polarisation unchanged: polarisation is not a vector, but a direction without a sense (though, of course, it is a consequence of the vector nature of light). And the turn, in the same sense as each unpolarised point is encircled, means that the singularity index is +1/2, rather than −1/2. Since there are four unpolarised points, the total index on the sphere of sky directions is +2, consistent with the Poincaré–Hopf theorem [59]: any smooth direction field on a sphere must have index +2.

The quantitative description of the pattern is provided by representing the polarisation by a complex function of sky direction, with zeros at the four unpolarised points. The simplest such function is a quartic polynomial and leads to the following theory [55]. The sky direction corresponding to elevation $\theta$ and azimuth $\phi$ is also represented, in stereographic projection, by a complex number:

$$\zeta = x + \mathrm{i}y = \frac{\left(1 - \tan\frac{1}{2}\theta\right)}{\left(1 + \tan\frac{1}{2}\theta\right)}\exp(\mathrm{i}\phi). \qquad (37)$$

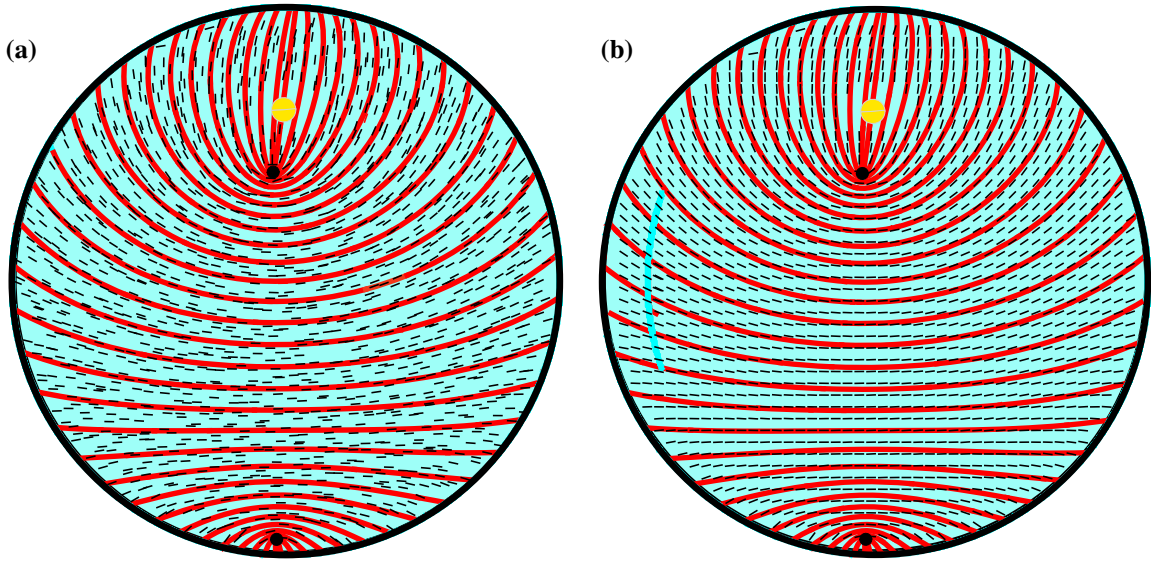


Figure 12. Line segments: observed directions of polarised daylight in the day sky; full curves: theory (39). (a) Line segments randomised within each cell of the measurement grid. (b) Line segments before randomisation, as originally published [55].

In this projection of the sky onto a plane, the visible hemisphere is represented by the unit disc whose centre is the zenith and boundary is the horizon. For sun elevation $\alpha$ and splitting $\delta$ of each singularity pair, we define

$$y_s = \frac{\left(1-\tan\frac{1}{2}\alpha\right)}{\left(1+\tan\frac{1}{2}\alpha\right)}, \quad A = \tan\frac{1}{4}\delta, \quad \zeta_t = \frac{\zeta + \mathrm{i}y_s}{1+\mathrm{i}\zeta y_s}. \quad (38)$$

Then, there is a function $f(x, y)$ whose contours are parallel to the polarisation direction at the sky point $(x, y)$, namely

$$f(x,y) = \mathrm{Im}\int^{\zeta_t} \frac{\mathrm{d}u}{\sqrt{-(u^2+A^2)(u^2+A^{-2})}} = A\mathrm{Im}F\left(\sin^{-1}\left(\frac{\mathrm{i}\zeta_t}{A}\right), A^2\right), \quad (39)$$

in which $F$ is the Legendre elliptic integral of the first kind [44]. As Figure 12(a) illustrates, this theory, based on *the elliptic integral in the sky*, gives a very accurate description of the observed polarisation pattern.

Unfortunately, the picture published in the paper [55] reporting the theory and experiment was not Figure 12(a) but Figure 12(b), which looks rather different. In fact, both pictures represent exactly the same data. In Figure 12(b), the experimental line segments representing the polarisation directions are centred on the point of the rectangular grid on which they were measured; the eye is drawn to the grid, rather than the directions of the line segments. A simple way to eliminate this misleading perception (understood only after Figure 12(b) was published) is to randomise the positions of the line segments within each unit cell of the grid. The result is Figure 12(a): the grid is no longer visible, and the agreement between theory and experiment is much clearer.

An interesting and controversial speculation [60,61] is that the Vikings, in their tenth-century voyages between Norway, Iceland and what is now Canada, might have used the sky polarisation pattern in conjunction with natural birefringent crystals (e.g. Iceland spar), as an aid to navigation.

## 8. Light in crystals: Hamilton's cone

Many natural transparent crystals are optically anisotropic and so are obvious materials for light to exhibit its polarisation properties. In each direction in such a crystal, two plane waves can travel, with orthogonal polarisations and different refractive indices [62]. A polar plot of the refractive indices in direction space generates the two-sheeted 'Fresnel wave surface', or, as we would call it now, the momentum-space contour surfaces of the Hamiltonians governing each of the two waves. In the most general crystals, all three principal dielectric constants are different, and, as Hamilton discovered [63,64], they intersect at four points on two 'optic axes'. The intersections take the form of double cones (diabolos).

There is beautiful physics associated with Hamilton's cones. In 1830, Hamilton himself made the first physical prediction based on his concept of phase space: that light incident on a thick slab of crystal along an optic axis would spread into a cone and emerge as a hollow cylinder. The immediate experimental observation of 'conical refraction' by his colleague Lloyd [65–67] created a sensation and brought instant fame to the young Hamilton. This story is described elsewhere [68], together with its modern developments.

A different (and more easily reproduced) demonstration of the cone geometry is illustrated in Figure 13. This shows the diffuse light of the sky viewed through a 'black light sandwich' [69]. The 'bread' consists of two crossed polarising sheets, and would allow no light to pass if there were nothing between them. But between the sheets is the 'filling' of the sandwich, consisting of a sheet of overhead projector transparency film: a material which, though not crystalline, is biaxially anisotropic. The simplest theory explaining the 'conoscopic' Figure 13 is the following.

Light passing through the transparency 'crystal' in directions, close to the optic axis, specified by coordinates $(x, y) = r(\cos\phi, \sin\phi)$ and propagating along $z$, can be described by a two-component vector $|\psi\rangle$ representing the linear polarisation amplitudes along directions perpendicular to $z$. The evolution of the polarisation as the light passes through the transparency, whose thickness is $l$, is determined by a Schrödinger-lookalike equation, written for wavenumber $k$,

$$\frac{\mathrm{i}}{k}\partial_z|\psi\rangle = \hat{H}|\psi\rangle, \quad \hat{H} = \begin{pmatrix} y & x \\ x & -y \end{pmatrix} = r\begin{pmatrix} \cos\phi & \sin\phi \\ \sin\phi & -\cos\phi \end{pmatrix} \quad 0 \leqslant z \leqslant l. \quad (40)$$

The Hamiltonian $\hat{H}$ describes the light in direction $(x, y)$, whose eigenvalues $\pm r$ describe the refractive index diabolo, and the eigenvectors are the orthogonal polarizations

$$\hat{H}|\pm\rangle = \pm r|\pm\rangle, \quad |+\rangle = \begin{pmatrix} \cos\frac{1}{2}\phi \\ \sin\frac{1}{2}\phi \end{pmatrix}, \quad |-\rangle = \begin{pmatrix} \sin\frac{1}{2}\phi \\ -\cos\frac{1}{2}\phi \end{pmatrix}. \quad (41)$$

Passing through the sandwich in the sequence 'polarizer-propagation-analyzer' is formally analogous to the sequence 'preparation-evolution-measurement' for quantum states, and the resulting direction-dependent intensity, representing the view through the sandwich, is

Figure 13. Bull's eye in the sky above Bristol, photographed through a black light sandwich: biaxially anisotropic overhead-transparency foil between crossed polarizers.

$$I(x,y) = \left|\langle \text{analyzer}|\text{propagation matrix } \exp\left(-\text{ik}l\hat{H}\right)|\text{polarizer}\rangle\right|^2 = \left|\begin{pmatrix}0 & 1\end{pmatrix}\begin{pmatrix}\cos lr - \text{i}y\frac{\sin klr}{r} & -\text{i}x\frac{\sin klr}{r} \\ -\text{i}x\frac{\sin klr}{r} & \cos lr + \text{i}y\frac{\sin klr}{r}\end{pmatrix}\begin{pmatrix}1\\0\end{pmatrix}\right|^2 = \frac{x^2\sin^2 klr}{r^2}. \quad (42)$$

This clearly explains Figure 13. The $\sin^2$ factor describes circular interference fringes as the loci of constant separation of the sheets of the diabolo, centred on the 'bull's eye' where the two indices are degenerate. The $(x/r)^2$ factor describes the vertical black 'brush', which is ultimately a consequence of the half-angles in (41), according to which the eigenpolarizations change sign ($\pi$ phase change) in a circuit of the optic axis $r = 0$.

I regard this $\pi$-phase change, observed in Lloyd's 1831 conical refraction experiment, as the first *geometric phase*, anticipating all of those being studied today [70,71]. And Hamilton's cone is the prototype of all the *conical intersections* now being studied in theoretical chemistry [72] and condensed matter physics, and popularly referred to as 'Dirac cones' [73]. In my opinion, this is a misnomer: Dirac never drew or even mentioned cones in this context, and the linear dependence of eigenvalues on momentum, leading to the Dirac equation, is exactly the geometry that Hamilton emphasised in the1830s.

Conoscopic figures, like Figure 13, are familiar to mineralogists. Several new intensity patterns have been predicted [74], but not yet observed, for crystals that are chiral and anisotropically absorbing as well as biaxially birefringent, and with different combinations of polarizer and analyzer.

## 9. The squint moon: a projection illusion

It is possible to see the sun and moon in the sky simultaneously at different periods of the day during each month, provided the sky is clear. The part of the moon's disc that we see, waxing from crescent to half to gibbous as the moon's phase changes from new to full, corresponds to our view of the hemisphere that is lit by the sun (Figure 14(a)). Therefore, we might expect the normal to the lit face (i.e. the normal to the line joining the horns of the moon) to point towards the sun. But it does not: the lit face points above the sun, to an extent that increases between new moon and full moon. This is the unexpected and striking 'squint moon' phenomenon [75–77]. Its explanation is a combination of geometry and perception.

It is obvious that in three-dimensional space, the normal to the lit hemisphere points directly to the sun. Therefore, the squint must be an illusion. It has alternatively been called the *New* Moon Illusion [78], to distinguish it from the unrelated more familiar moon illusion in which the moon appears large near the horizon. The squint illusion can be immediately dispelled [3] by stretching a string taut close to the eye and orienting it from the moon to the sun.

To understand the illusion, we first note that the sun and moon are too distant for our stereoscopic vision to

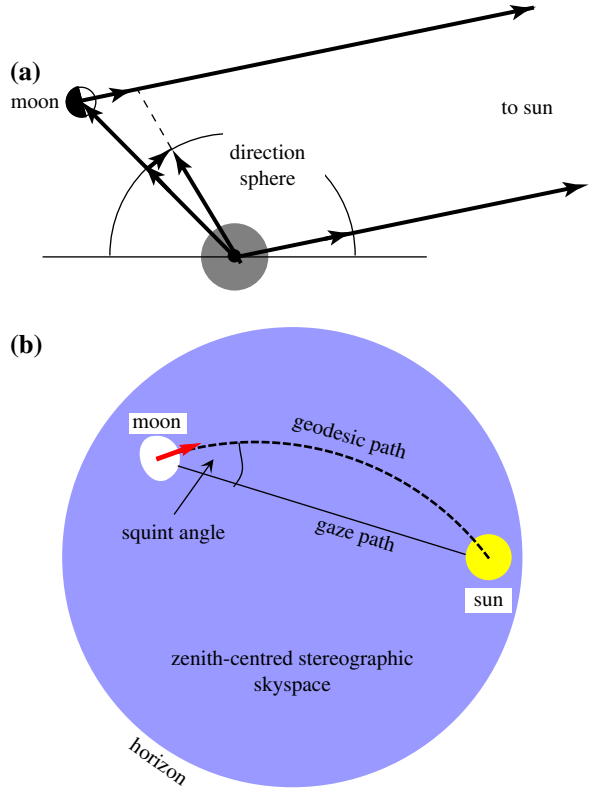


Figure 14. (a) Moon–sun geometry in space and on the direction sphere. (b) Simulation of the squint moon as seen in 'skyspace', modelled by zenith-centred stereographic projection from the direction sphere.

operate, so we cannot perceive their arrangement in three-dimensional space. We cannot see distances; all we can perceive are directions. Each direction can be regarded as a point on an earth- (or eye-) centred unit sphere. On this sphere, the straight line in space joining the sun and moon projects onto a great circle: a geodesic curve. But we do not perceive this sphere directly. Instead, we see objects in the sky, and relations between them, as though projected onto an imaginary screen, roughly flat. Call this 'skyspace'. The squint moon illusion is related to the projection from the direction sphere onto skyspace.

I do not know which projection our visual system chooses, or even if it is the same at different times and for different people. But the illusion is remarkably stable against the change from one projection to another. To illustrate this, Figure 14(b) shows the stereoscopic projection of skyspace according to (37), mimicking how we might see the sky when lying on our back looking up. The squint is very clear: the geodesic connecting the moon and sun on the direction sphere projects onto a circular arc in skyspace, whose tangent at the position of the moon points in a different direction to the straight 'gaze path' from the moon to the sun in skyspace.

Zenith-centred stereographic projection is particularly interesting because on this skyspace the horizon is curved; yet the squint is strong, apparently contradicting claims [75] that the illusion depends on seeing the horizon as straight. It would be interesting to see if the squint persists in space far above the earth, where there is no horizon.

In most skyspaces, geodesics on the direction sphere appear projected as curves; stereographic projection is just one example. But Professor Zeev Vager (personal communication) points out an important class of projections for which great circles on the sphere appear as straight lines, namely the perspective ('pinhole') projections. For these skyspaces, the squint arises because perspective does not preserve angles: it is not conformal. In particular, the angle in skyspace, between the horns of the moon and the (now straight) line from the sun to the moon, is not 90°.

## 10. Concluding remarks: the sky as an optics laboratory

It should be clear from my eclectic series of examples that natural optical phenomena illustrate, and have been implicated in the development of, a surprisingly large number of scientific concepts:

- *Caustics* – the singularities of geometrical optics – are central to understanding rainbows, mirages, and the sparkling of light on water.
- *Numerical experiments* played a central part in understanding both the ray and wave aspects of rainbows. Replacing numerical experiments by analysis led to a seminal insight into
- *Mathematical asymptotics*, still being developed now, with new classes of applications.
- *Dispersion* explains the green flash, as well as the rainbow colours in geometrical optics.
- *Complex angular momentum*, in the form of
- *Regge poles*, supplied the key to understanding the glory. Several numerical
- *Coincidences* underlie the comparable brightnesses of the two earthlights on the moon (less familiar than the coincidentally similar angular sizes of the sun and moon, responsible for the spectacle of the solar eclipse).
- The blue day sky and natural crystals exhibit the *Polarisation singularities* being intensively explored as one of the pillars of singular optics.
- *Geometric phases* and
- *Conical intersections* first appeared in crystal optics. And the squint moon exemplifies the
- *Geometry of visual illusions* that mislead our perception.

## Acknowledgements

I thank Professor Roy Bishop for permission to reproduce Figure 1, Professor Zeev Vager and Mr. Omer Abramson for introducing me to the squint moon illusion and a helpful correspondence, Professor Andrew Young for advice on mirages, and Professors Mark Dennis and Pragya Shukla for their careful readings of the first draft and helpful suggestions.

## Notes on contributor

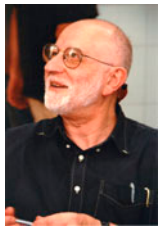

Sir M.V. Berry is a theoretical physicist at the University of Bristol, where he has been for nearly twice as long as he has not. His research centres on the relations between physical theories at different levels of description (classical and quantum physics, and ray optics and wave optics). He delights in finding familiar phenomena illustrating deep concepts: the arcane in the mundane.



## References

[1] J.M. Pernter and F.M. Exner, *Meterologische Optik*, W. Braunmüller, Wien, 1922.
[2] R.A.R. Tricker, *Introduction to Meteorological Optics*, Elsevier, New York, 1970.
[3] M. Minnaert, *The Nature of Light and Colour in the Open Air*, Dover, New York, 1954.
[4] R. Greenler, *Rainbows, Halos and Glories*, University Press, Cambridge, 1980.
[5] D.K. Lynch and W. Livingston, *Color and Light in Nature*, University Press, Cambridge, 1995.
[6] R. Lee and A. Fraser, *The Rainbow Bridge: Rainbows in Art, Myth and Science*, Pennsylvania State University and SPIE press, Bellingham, WA, 2001.
[7] C.B. Boyer, *The Rainbow from Myth to Mathematics*, Princeton University Press, Princeton, NJ, 1987.
[8] D. Park, *The Fire within the Eye: A Historical Essay on the Nature and Meaning of Light*, University Press, Princeton, NJ, 1997.
[9] M.V. Berry and C. Upstill, *Catastrophe optics: morphologies of caustics and their diffraction patterns*, Prog. Opt. 18 (1980), pp. 257–346.
[10] T. Young, *The Bakerian lecture: on the theory of light and colours*, Phil. Trans. Roy. Soc. 92 (1802), pp. 12–48.
[11] T. Young, *The Bakerian lecture: experiments and calculations relative to physical optics*, Phil. Trans. Roy. Soc. Lond. 94 (1804), pp. 1–16.
[12] M.V. Berry, *Exuberant interference: rainbows, tides, edges, (de)coherence*, Phil. Trans. Roy. Soc. Lond. A 360 (2002), pp. 1023–1037.
[13] G.B. Airy, *On the intensity of light in the neighbourhood of a caustic*, Trans. Camb. Phil. Soc. 6 (1838), pp. 379–403.
[14] H.M. Nussenzveig, *Diffraction Effects in Semiclassical Scattering*, University Press, Cambridge, 1992.
[15] G.G. Stokes, *On the numerical calculation of a class of definite integrals and infinite series*, Trans. Camb. Phil. Soc. 9 (1847), pp. 379–407.
[16] G.G. Stokes, *On the discontinuity of arbitrary constants which appear in divergent developments*, Trans. Camb. Phil. Soc. 10 (1864), pp. 106–128.
[17] G.G. Stokes, *On the discontinuity of arbitrary constants that appear as multipliers of semi-convergent series*, Acta Math. 26 (1902), pp. 393–397.
[18] M.V. Berry, *Uniform asymptotic smoothing of Stokes's discontinuities*, Proc. Roy. Soc. Lond. A422 (1989), pp. 7–21.
[19] M.V. Berry, *Stokes' phenomenon; smoothing a Victorian discontinuity*, Publ. Math. Institut des Hautes Études scientifique 68 (1989), pp. 211–221.
[20] M.V. Berry, *Asymptotics, superasymptotics, hyperasymptotics*, in *Asymptotics Beyond All Orders*, H. Segur and S. Tanveer, eds., Plenum, New York, 1992, pp. 1–14.
[21] M.V. Berry and C.J. Howls, *Divergent series: taming the tails*, in *The Princeton Companion to Applied Mathematics*, N. Higham, ed., University Press, Princeton, NJ, 2015, in press.
[22] R.B. Dingle, *Asymptotic Expansions: their Derivation and Interpretation*, Academic Press, New York, 1973.
[23] M.V. Berry and C.J. Howls, *Hyperasymptotics*, Proc. Roy. Soc. Lond. A430 (1990), pp. 653–668.
[24] M.V. Berry and C.J. Howls, *Hyperasymptotics for integrals with saddles*, Proc. Roy. Soc. Lond. A434 (1991), pp. 657–675.
[25] G.V. Dunne and M. Ünsal, Uniform WKB, multi-instantons, and resurgent trans-series, Phys. Rev. D 89 (2014), p. 105009.
[26] R.L. Lee, *What are 'all the colors of the rainbow'?* Appl. Opt. 30 (1991), pp. 3401–3407.
[27] C. Chester, B. Friedman, and F. Ursell, *An extension of the method of steepest descents*, Proc. Camb. Phil. Soc. 53 (1957), pp. 599–611.
[28] M.V. Berry, *Uniform approximation for potential scattering involving a rainbow*, Proc. Phys. Soc. 89 (1966), pp. 479–490.
[29] R. Wong, *Asymptotic Approximations to Integrals*, Academic Press, New York, 1989.
[30] K.W. Ford and J.A. Wheeler, *Semiclassical description of scattering*, Ann. Phys. (NY) 7 (1959), pp. 259–286.
[31] K.W. Ford and J.A. Wheeler, *Application of semiclassical scattering analysis*, Ann. Phys. (NY) 7 (1959), pp. 287–322.
[32] M.V. Berry, *Cusped rainbows and incoherence effects in the rippling-mirror model for particle scattering from surfaces*, J. Phys. A 8 (1975), pp. 566–584.
[33] M.V. Berry and C.J. Howls, *Integrals with coalescing saddles*. Chapter 36, in *NIST Digital Library of Mathematical Functions*, F.W.J. Olver, D.W. Lozier R.F. Boisvert and C.W. Clark, eds., University Press, Cambridge, 2010, pp. 775–793.
[34] J.F. Nye, *Natural Focusing and Fine Structure of Light: Caustics and Wave Dislocations*, Institute of Physics Publishing, Bristol, 1999.
[35] M.S. Longuet-Higgins, *Reflection and refraction at a random moving surface. I. Pattern and paths of specular points*, J. Opt. Soc. Amer. 50 (1960), pp. 838–844.
[36] M.S. Longuet-Higgins, *Reflection and refraction at a random moving surface. II. Number of specular points in a Gaussian surface*, J. Opt. Soc. Amer. 50 (1960), pp. 845–850.
[37] M.S. Longuet-Higgins, *Reflection and refraction at a random moving surface. III. Frequency of twinkling in a Gaussian surface*, J. Opt. Soc. Amer. 50 (1960), pp. 851–856.
[38] M.V. Berry and M.R. Dennis, *Phase singularities in isotropic random waves*, Proc. Roy. Soc. A 456 (2000), pp. 2059–2079, corrigenda in A456 p3048.

[39] M.V. Berry and M.R. Dennis, *Polarization singularities in isotropic random vector waves*, Proc. Roy. Soc. Lond. A457 (2001), pp. 141–155.
[40] A.T. Young, *An introduction to mirages*, 2012. Available at: http://mintaka.sdsu.edu/GF/mirages/mirintro.html.
[41] M.V. Berry, *Raman and the mirage revisited: confusions and a rediscovery*, Eur. J. Phys. 34 (2013), pp. 1423–1437.
[42] DLMF, *NIST Handbook of Mathematical Functions,* University Press, Cambridge, 2010. Available at: http://dlmf.nist.gov.
[43] W. Tape, *The topology of mirages*, Sci Am. 252 (1985), pp. 120–129.
[44] M.V. Berry, *Disruption of images: the caustic-touching theorem*, J. Opt. Soc. Amer. A4 (1987), pp. 561–569.
[45] D.J.K. O'Connell, *The Green Flash and Other Low Sun Phenomena*, Vatican Observatory, Rome, 1958.
[46] A.T. Young, *Annotated bibliography of atmospheric refraction, mirages, green flashes, atmospheric refraction, etc.*, 2012. Available at: http://mintaka.sdsu.edu/GF/bibliog/bibliog.html.
[47] H.C. van de Hulst, *Light Scattering by Small Particles*, Dover, New York, 1981.
[48] C.F. Bohren and A.B. Fraser, *At what altitude does the horizon cease to be visible?* Am. J. Phys. 54 (1986), pp. 222–227.
[49] H.M. Nussenzveig, *High-frequency scattering by a transparent sphere. II. Theory of the rainbow and the Glory*, J. Math. Phys. 10 (1969), pp. 125–176.
[50] R. Lenke, U. Mack, and G. Maret, *Comparison of the 'glory' with coherent backscattering of light in turbid media*, J. Opt. A 4 (2002), pp. 309–314.
[51] C.M. Aegerter and G. Maret, *Coherent backscattering and Anderson localization of light*, Prog. Opt. 52 (2009), pp. 1–62.
[52] H.M. Nussenzveig, *High-frequency scattering by a transparent sphere. I. Direct reflection and transmission*, J. Math. Phys. 10 (1969), pp. 82–124.
[53] G. Horvath, J. Gal, and I. Pomozi, *Polarization portrait of the Arago point: video-polarimetric imaging of the neutral points of skylight polarization*, Naturwiss 85 (1998), pp. 333–339.
[54] G. Horváth, B. Bernáth, B. Suhai, and A. Barta, *First observation of the fourth neutral polarization point in the atmosphere*, J. Opt. Soc. Amer. A. 19 (2002), pp. 2085–2099.
[55] M.V. Berry, M.R. Dennis, and R.L.J. Lee, *Polarization singularities in the clear sky*, New J. Phys. 6 (2004), p. 162.
[56] S. Chandrasekhar and D. Elbert, *Polarization of the sunlit sky*, Nature 167 (1951), pp. 51–55.
[57] S. Chandrasekhar and D. Elbert, *The illumination and polarization of the sunlit sky on Rayleigh scattering*, Trans. Amer. Philos. Soc. 44 (1954), pp. 643–728.
[58] J.H. Hannay, *Polarization of sky light from a canopy atmosphere*, New. J. Phys 6 (2004), p. 197.
[59] V. Guillemin and A. Pollack, *Differential Topology*, Prentice-Hall, Englewood Cliffs, NJ, 1974.
[60] R. Hegedüs, S. Åkesson, R. Wehner, and G. Horváth, *Could Vikings have navigated under foggy and cloudy conditions by skylight polarization? On the atmospheric optical prerequisites of polarimetric Viking navigation under foggy and cloudy skies*, Proc. Roy. Soc. A 463 (2007), pp. 1081–1095.
[61] L.K. Karlsen, *Secrets of the Viking Navigators*, One Earth Press, Seattle, WA, 2003.
[62] M. Born and E. Wolf, *Principles of Optics*, Pergamon, London, 2005.
[63] W.R. Hamilton, *Third supplement to an essay on the theory of systems of rays*, Trans. Roy. Irish. Acad. 17 (1837), pp. 1–144.
[64] J.G. Lunney and D. Weaire, *The ins and outs of conical refraction*, Europhysics News 37 (2006), pp. 26–29.
[65] H. Lloyd, *On the phaenomena presented by light in its passage along the axes of biaxial crystals*, Phil. Mag. 2 (1833), pp. 112–120 and 207–210.
[66] H. Lloyd, *Further experiments on the phaenomena presented by light in its passage along the axes of biaxial crystals*, Phil. Mag. 2 (1833), pp. 207–210.
[67] H. Lloyd, *On the phenomena presented by light in its passage along the axes of biaxial crystals*, Trans. Roy. Irish. Acad. 17 (1837), pp. 145–158.
[68] M.V. Berry and M.R. Jeffrey, *Conical diffraction: Hamilton's diabolical point at the heart of crystal optics*, Prog. Opt. 50 (2007), pp. 13–50.
[69] M.V. Berry, R. Bhandari, and S. Klein, *Black plastic sandwiches demonstrating biaxial optical anisotropy*, Eur. J. Phys. 20 (1999), pp. 1–14.
[70] M.V. Berry, *Quantal phase factors accompanying adiabatic changes*, Proc. Roy. Soc. Lond. A392 (1984), pp. 45–57.
[71] A. Shapere and F. Wilczek, *Geometric Phases in Physics*, World Scientific, Singapore, 1989.
[72] L.S. Cederbaum, R.S. Friedman, V.M. Ryaboy, and N. Moiseyev, *Conical intersections and bound molecular states embedded in the continuum*, Phys. Rev. Lett 90 (2003), pp. 013001-1-4.
[73] E. Kalesaki, C. Delerue, C. Morais Smith, W. Beugeling, G. Allan, and D. Vanmaekelbergh, *Dirac cones, topological edge states, and nontrivial flat bands in two-dimensional semiconductors with a honeycomb nanogeometry*, Phys. Rev. X 4 (2014), p. 011010.
[74] M.V. Berry and M.R. Dennis, *The optical singularities of birefringent dichroic chiral crystals*, Proc. Roy. Soc. A. 459 (2003), pp. 1261–1292.
[75] B. Schölfopf, *The moon tilt illusion*, Perception 27 (1998), pp. 1229–1232.
[76] H.J. Schlichting, *Schielt der Mond?* Spektrum der Wissenschaft (2012), pp. 56–58.
[77] G. Glaeser and K. Schott, *Geometric considerations about seemingly wrong tilt of crescent moon*, KoG (Croatian Soc. Geom. Graph.) 13 (2009), pp. 19–26.
[78] B.J. Rogers and S.M. Anstis, *The new moon illusion*, in *The Oxford Compendium of Visual illusions*, A.G. Shapiro and D. Todorovic, eds., Oxford University Press, New York and Oxford, 2014, in press.